Insights into the statistical γ-decay behavior of ^{108}Cd via radiative proton capture

F. Heim,* P. Scholz, M. Körschgen, J. Mayer, M. Müller, and A. Zilges
Institute for Nuclear Physics, University of Cologne, 50937 Köln, Germany

(Received 18 September 2018; revised manuscript received 28 February 2020; accepted 3 March 2020; published 17 March 2020)

Background: For the description of many astrophysical processes, precise knowledge of cross sections and reaction rates is necessary. In particular, the exact nucleosynthesis mechanisms of the p nuclei—a group of 30 to 35 neutron deficient nuclei—are still unknown. Since many reactions of astrophysical relevance are not accessible in the laboratory, one has to rely on theoretical calculations based on Hauser-Feshbach codes. The calculated values depend strongly on nuclear physics input parameters like nuclear level densities (NLDs), γ-ray strength functions (γ-SFs) and particle+nucleus optical model potentials (OMPs).
Purpose: Measuring the ^{107}Ag$(p,\gamma)^{108}$Cd reaction cross section at sub-Coulomb energies extends the scarce experimental database. In particular, partial cross sections yield important information about the γ-SF in ^{108}Cd. Via the comparison of total (p,γ) cross sections to theoretical calculations, a locally adopted NLD model was found.
Method: Highly enriched ^{107}Ag targets were bombarded with protons at six different beam energies between 2.0 and 5.0 MeV. The reaction yield and thus the reaction cross section were determined via in-beam γ-ray spectroscopy using the HORUS γ-ray spectrometer. Total (p,γ) cross sections were obtained by the observation of ground-state transitions in ^{108}Cd and partial cross sections via the analysis of primary γ-ray transitions into different excited states in ^{108}Cd.
Results: Cross-section values at six energies close to the astrophysical relevant energy region were determined. The slight adjustment of microscopic models for the NLD to the total (p,γ) cross sections, respectively the dipole strength function to the partial cross sections, yielded an excellent agreement between the experimentally determined results and statistical model calculations.
Conclusion: The obtained results help to constrain the nuclear physics input for statistical model calculations and hence to improve the precision of the theoretical determination of reaction rates. In particular, information about the p nucleus ^{108}Cd helps us to understand the mechanisms of the p process.

DOI: 10.1103/PhysRevC.101.035805

I. INTRODUCTION

The majority of heavier nuclei beyond the iron peak are synthesized either via the slow neutron-capture process (s process) or the rapid neutron-capture process (r process) [1–4]. A group of 30 to 35 stable neutron deficient nuclei are bypassed by those processes—the p nuclei [5–9]. Their isotopic abundances relative to other isotopes of the same element amount to only about 1% except for the light p nuclei ^{92,94}Mo and ^{96,98}Ru, and ^{144}Sm [10]. The detailed explanation of their abundances remains one of the biggest puzzles relating to the p process.

Today, the p process does not denote one single reaction path, but several processes that are able to produce the p nuclei. The largest contribution to their synthesis is assumed to stem from the so-called γ process [8,11,12] which occurs in any sufficiently hot plasma. It was first explored in simulations of massive star explosions [13,14] but was also recently investigated in type Ia supernovae [15]. According to this concept, in an explosive astrophysical scenario temperatures between about 2 and 3 GK are reached and therefore s or r seed nuclei can be photodissociated. A range of temperatures is needed to allow the synthesis of the p nuclei within the γ process. While nuclei of lower masses require higher temperatures for photodisintegration (2.5–3.5 GK), heavier nuclei should not be exposed to very high temperatures (<2.5 GK) as otherwise the newly synthesized nuclei tend to be destroyed immediately [16]. Branching points where the γ process path can be deflected towards other isotopic chains are determined by the probabilities of (γ,p) and (γ,α) reactions.

A further contribution stems from the rapid proton-capture (rp) process which most likely occurs in type I x-ray bursts [17,18]. In this scenario high temperatures of about 0.5 GK can be reached and an increasing leakage out of the CNO cycle is initiated by the ^{15}O$(\alpha,\gamma)^{19}$Ne reaction [19]. Given the right conditions for temperature and density, a flow towards the region of proton-unbound nuclei along an isotonic chain is possible and so is the nucleosynthesis of certain p nuclei. The nucleosynthesis of heavier p nuclei may partly be explained by the νp process: strong neutrino flows acting on the hot matter of core-collapse supernovae induce the $\bar{\nu}_e + p \rightarrow n + e^+$

*fheim@ikp.uni-koeln.de

reaction producing free neutrons which then induce (n, p) reactions on proton rich nuclei, created, e.g., within the rp process. Thus, matter is driven back towards the valley of stability and further proton captures are possible [20].

In general, different processes and mechanisms do not contribute independently of each other to the synthesis of all kind of elements but can interlock fluently within various astrophysical scenarios. Further information and an overview of the nuclear processes in the universe can be found in Ref. [21].

Not only within the γ process and the nucleosynthesis of p nuclei but in all processes related to nucleosynthesis a large number of (mostly unstable) nuclei and nuclear reactions are involved. For most of those, detailed nuclear information is neither available nor accessible in the laboratory, hence for many properties one has to rely completely on theoretical models. In particular, cross sections and reaction rates at astrophysical energies, i.e., far below the Coulomb barrier, need to be extrapolated using theoretical calculations. Further information can be found in Refs. [21,22].

For this purpose the Hauser-Feshbach statistical model is widely used [23,24]. The uncertainties in its predictions are basically dominated by the uncertainties in nuclear physics input parameters such as γ-ray strength functions (γ-SFs), nuclear level densities (NLDs), and particle+nucleus optical-model potentials (OMPs) [8,25]. At energies achievable in experiments, radiative capture reaction cross sections are usually very sensitive to the γ width, which is composed of the γ-strength function and nuclear level densities [8,9,25]. In general, proton- and neutron optical-model potentials are much better studied than, e.g., the α-OMP (see Refs. [26,27] and references therein).

The present work focuses on the determination of total and partial cross sections of the ^{107}Ag(p, γ) reaction for proton beam energies between 2.0 and 5.0 MeV. The motivation for this experiment is twofold: First, the measurement of the cross sections helps to enlarge the experimental database related to the γ process and, therefore, to describe the synthesis of p nuclei. Second, detailed studies of the γ-SF and NLD in the p nucleus ^{108}Cd are feasible via total and partial cross-section measurements [28,29]. Hence, we not only extend the experimental database regarding the pure cross sections, but also deliver major information about the underlying nuclear structure. The latter is essential for reliable and robust network calculations.

The analysis of the ^{107}Ag$(p, \gamma)^{108}$Cd reaction has been carried out utilizing the in-beam γ-ray spectroscopy method [26,28,30,31]. In contrast to the activation technique (see, e.g., Refs. [27,32]), this method offers the opportunity to study reactions with stable product nuclei. Total (p, γ) cross-section values (in the following called total cross section) of radiative proton-capture reactions are very sensitive to the NLD and, therefore, those measurements can help to either constrain or exclude certain NLD models. Results for partial cross-section values are dominated by the γ-SF. Hence, those measurements allow one to study properties of the γ-decay behavior in ^{108}Cd. The long-term goal is to find robust models for these nuclear properties which allow precise and reliable predictions of cross sections and reaction rates, even when going away from stability or at very low or high energies.

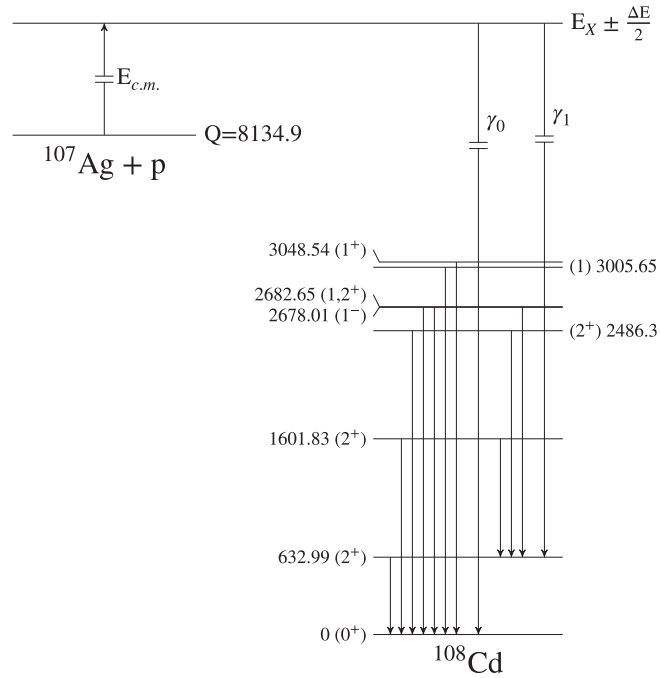

FIG. 1. Illustration of the reaction mechanism that leads to the highly excited compound nucleus after a radiative-capture reaction. The compound state contains numerous unresolved resonances and has a width of $\frac{\Delta E}{2}$, with the energy loss ΔE. It then deexcites either directly into the ground state of ^{108}Cd (γ_0) or into various excited levels (γ_1, γ_2, and so on). Only states which can deexcite at least partly into the ground state are shown. All data were taken from [34].

In Sec. II a brief summary of the experimental setup and method is given, followed by an overview of the data analysis in Sec. V. In Secs. IV and V our experimental results as well as the comparison to statistical model calculations using TALYS [33] are given. This includes a short introduction of the mechanisms of Hauser-Feshbach calculations and their main nuclear ingredients.

II. EXPERIMENTAL SETUP AND METHOD

The in-beam technique was used to measure the ^{107}Ag$(p, \gamma)^{108}$Cd reaction since the end product ^{108}Cd is stable. After the bombardment of the target nucleus with protons of energy E_p, a highly excited compound nucleus is formed with an excitation energy of $E_x = Q + E_{\text{c.m.}}$. The Q value of the reaction is +8135 keV. Figure 1 shows a schematic illustration of the reaction mechanism and the subsequent γ decay of the compound nucleus.

Using the in-beam technique with high-purity germanium (HPGe) detectors, *total cross sections* can be derived from measuring all γ-ray transitions into the ground state (g.s.) of ^{108}Cd, whereas *partial cross sections* denote the probability for a capture and decay into an excited state of ^{108}Cd.

Photons from the decay of the excited compound nucleus are not emitted isotropically but with an angular distribution

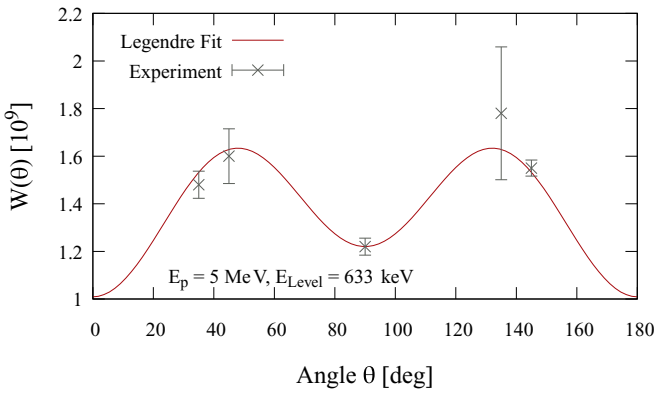

FIG. 2. Angular distribution of the γ decay $2_1^+ \rightarrow$ g.s. in ^{108}Cd for an incident beam energy of 5 MeV. A sum of Legendre polynomials is fitted to the data points in order to obtain the total number of reactions. Only one detector is mounted at an angle of 135° and therefore the statistical uncertainty for this angle is larger.

$W(\Theta)$ with respect to the beam axis. The experimental yield $Y(E_\gamma)$ is first corrected for the full-energy peak efficiency $\epsilon(E_\gamma)$ and the dead time correction of the data acquisition τ:

$$W(\Theta) = \frac{Y(E_\gamma)}{\epsilon(E_\gamma)\tau}. \quad (1)$$

At the HORUS γ-ray spectrometer, $Y(E_\gamma)$ is measured by up to 14 HPGe detectors, whereupon detectors covering the same angle are summed resulting in five different groups. The angular distribution is obtained by fitting a sum of Legendre polynomials to the five experimental values:

$$W(\Theta) = A_0\left(1 + \sum_{k=2,4} \alpha_k P_k(\cos\Theta)\right). \quad (2)$$

In this equation A_0 and α_k denote energy-dependent coefficients and P_k the Legendre polynomials P_2 and P_4. Taking only Legendre polynomials with $k \leqslant 4$ into account is justified by the assumption that dipole and quadrupole transitions dominate the reaction mechanisms. Those angular distributions are obtained for each γ-ray transition at each beam energy and the sum of all A_0 coefficients represents the total number of reactions. Figure 2 shows an example of the angular distribution for the decay $2_1^+ \rightarrow$ g.s. in ^{108}Cd ($E_\gamma = 633$ keV) for an incident proton energy of 5 MeV. The total cross section is then calculated using the angular distributions of all ground-state transitions:

$$\sigma(p,\gamma)_{\text{total}} = \frac{\sum_{i=1}^{N} A_0^i}{N_P N_T}, \quad (3)$$

assuming in total N ground-state transitions, and N_P and N_T are the numbers of projectiles and target nuclei per area, respectively.

All detector end caps were shielded with 2 mm copper plates and five detectors were equipped with bismuth germanate (BGO) shields for an active background suppression. Further background suppression is achieved by placing the target within a *cooling finger*, a copper tube surrounding the target and cooled by LN_2 to minimize residual gas deposits on the target material. Using this setup, a stable vacuum of the order of 10^{-6} to 10^{-7} mbar is reached. The beam current is read out at the target, the chamber, and a Faraday cup behind the target. To prevent δ electrons from escaping the chamber, a suppression voltage of -400 V is applied. A built-in silicon detector is used for Rutherford backscattering spectrometry (RBS) measurements to monitor the target during the experiment.

TABLE I. Details of deposited charge on the targets and resulting number of particles. For this in-beam cross-section measurement the mean current was between about 400 and 650 nA.

E_p (MeV)	Target	Time (h)	I_{mean} (nA)	N_p
2.0	3	154	634.6	2.19×10^{18}
2.7	3	138	497.9	1.54×10^{18}
3.5	5	103	592.8	1.37×10^{18}
4.0	2	117	603.1	1.58×10^{18}
4.5	4	120	584.4	1.57×10^{18}
5.0	1	145	416.8	1.35×10^{18}

III. DATA ANALYSIS

A. Beam intensity and energy

The ^{107}Ag$(p,\gamma)^{108}$Cd reaction was studied at six astrophysical relevant proton energies between 2.0 and 5.0 MeV. The Gamow window is between 1.77 and 3.83 MeV at $T = 3.0$ GK. Details of the irradiation can be found in Table I. Except for the proton energies of 2.0 and 2.7 MeV, a different target was used for each beam energy.

A precise determination of the particle beam energy is important. Therefore, the resonance of the ^{27}Al$(p,\gamma)^{28}$Si reaction at $E_p = 3674.4$ keV [35] was scanned in small energy steps (up to a few keV). The peak volume of the $4_1^+ \rightarrow 2_1^+$ transition in ^{28}Si at 2838 keV was normalized to the accumulated charge deposited on the target. The resulting resonance curve is shown in Fig 3. The width of the sharp rising edge

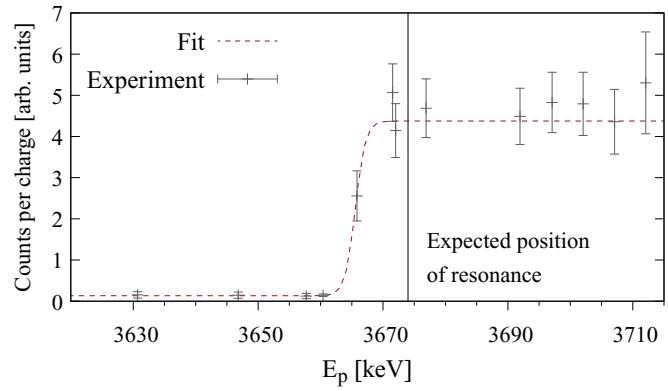

FIG. 3. Resonance curve of the ^{27}Al(p,γ) reaction. By normalizing the volume of the 2838 keV peak to the collected charge the energy of the incident protons can be determined. See text for details.

of the resonance curve is determined by the spread in energy of the proton beam. The width of the plateau is caused by the energy loss of the protons in the target. The results show that the actual beam energy is about 9 keV higher than expected with an energy spread of about 4 keV. It is generally assumed that those values neither change during the experiment nor vary with beam energy [30].

B. Target thickness and energy loss

The enrichment of the six ^{107}Ag targets was (99.5%). They were manufactured as self-supporting foils by rolling. A gold foil with thickness of 140 mg/cm^2 was used as backing to stop the beam. The thicknesses of the targets were determined via Rutherford backscattering spectrometry (RBS) at the RUBION facility in Bochum, Germany. The experimental results were compared to SIMNRA [36] simulations leaving the effective target thickness as a free parameter. Taking a thickness distribution and roughness on the surface into account, the simulation yields very good agreement with the experimental RBS spectra. Effective target thicknesses from 2.79×10^{18} to 3.45×10^{18} atoms/cm^2 were determined. The targets are favored to be thin enough to keep the energy loss small. This loss is estimated via SRIM [37], resulting in an average energy loss ΔE between 15 and 28 keV. The effective interaction energy of the protons is

$$E_p = E_0 + E_{\text{offset}} - \frac{\Delta E}{2}. \tag{4}$$

C. γ-ray detection procedure

The standard calibration sources ^{226}Ra and ^{60}Co as well as ^{56}Co were used for the low-energy efficiency calibration. Since primary γ-ray transitions from the compound state have γ-ray energies of around 10 MeV, a reliable full-energy efficiency up to this energy region is needed. For this, the resonance at $E_p = 3674.4$ keV of the ^{27}Al$(p,\gamma)^{28}$Si reaction [35] was used (see Fig. 3). The γ-branching ratios for the depopulation of the state at $E_x = 15\,127$ keV are known from Ref. [35]. The total full energy-peak efficiency amounts to about 3% and a resolution of FWHM $\approx$ 2 keV at a γ-ray energy of 1.3 MeV was determined.

A typical γ-ray spectrum for the beam energy of $E_p =$ 5000 keV is shown in Fig. 4. Since the target material was highly enriched, no significant contributions from contaminants are expected and, thus, clean spectra were obtained and are shown in the top panel of Fig. 4. The observed γ-ray transitions stem from ^{107}Ag, the (p,n) product ^{107}Cd, the (p,γ) product ^{108}Cd, the backing ^{197}Au, and ^{27}Al from which the chamber is made. Since the (p,n) threshold is at about 2200 keV, a heavily reduced background and a reduction of the number of peaks in the spectrum is visible for $E_p =$ 2000 keV [see Fig. 4(b)].

The bottom panel in Fig. 4 shows the deexcitation of the compound state into the ground state and various excited states in ^{108}Cd. Direct deexcitations up to the eighth excited state can be observed. However, the intensity of the different transitions decreases tremendously with beam energy. For a better identification, the spectra for all beam energies are

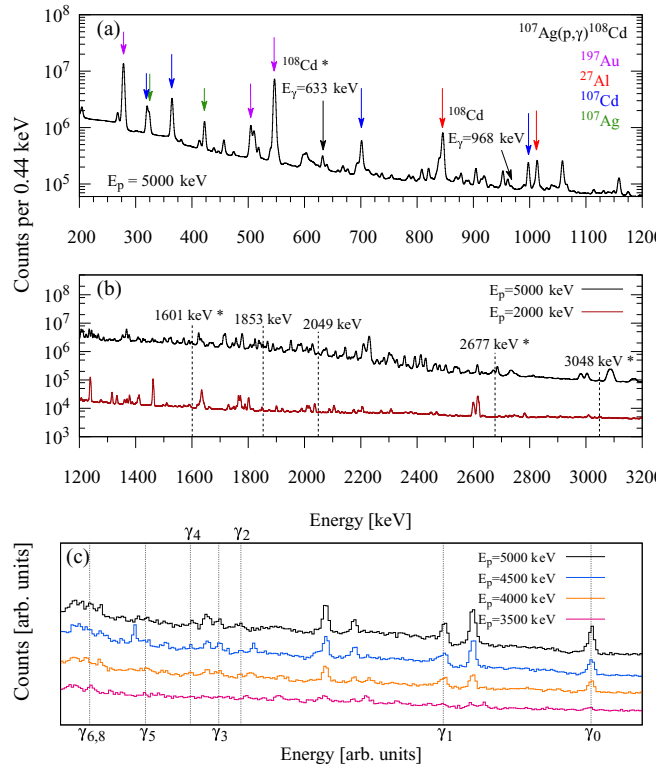

FIG. 4. Typical γ-ray spectrum for the ^{107}Ag$(p,\gamma)^{108}$Cd reaction. The top panel (a) shows the low-energy part of the spectrum. All strong peaks can be identified. Most of the transitions stem from the ^{107}Ag(p,n) reaction. Below the (p,n) threshold of $E_{th} =$ 2200 keV, the spectrum is much cleaner. This is shown in the middle panel (b). Direct g.s. transitions are marked with an asterisk (*). The high-energy part in (c) shows the deexcitation of the compound state to excited levels in ^{108}Cd. The energies of the primary transitions (γ_0, γ_1, and so on) depend on the beam energies. Hence, for better visualization the spectra are shifted and the x axis is given in arbitrary units.

shifted so that primary γ-ray transitions to the same final states match up. This means the spectrum for $E_p = 4500$ keV is shifted by 500 keV to higher energies and so on.

For the determination of total cross sections, the intensity of all ground-state (g.s.) transitions has to be calculated. In total, seven g.s. transitions were observed; however, some of those transitions were overlapping with background transitions (e.g., from ^{107}Cd). The branching into the 2_1^+ state at $E_\gamma = 633$ keV was analyzed in these cases instead. The intensity for the population of the ground state was then determined using the tabulated γ-branching ratio.

The HORUS γ-ray spectrometer combined with the digital data acquisition system allows the measurement of $\gamma\gamma$ coincidences, a very powerful tool to suppress beam-induced background [38]. The $\gamma\gamma$-coincidence technique helps for the identification of γ-ray transitions, as they can be assigned easily to a certain nucleus. An example of the $\gamma\gamma$-coincidence technique for this experiment is illustrated in Fig. 5. In the top panel the original spectrum for a proton energy of $E_p =$ 5000 keV is given. The spectrum shows many transitions and peaks, mainly from the (p,n) product ^{107}Cd or inelastic

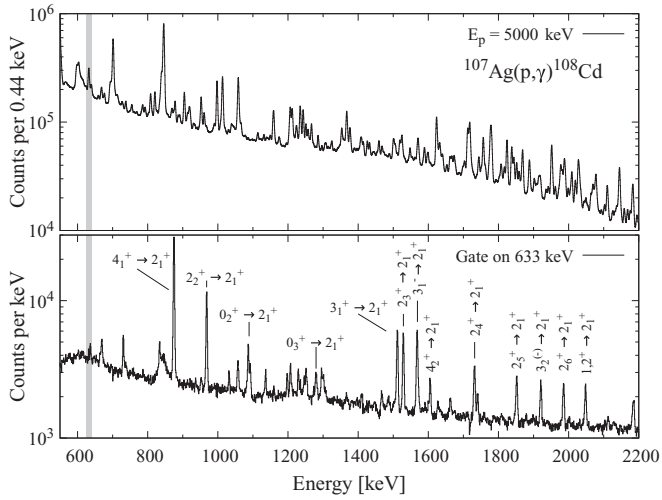

FIG. 5. Excerpt from a spectrum of the ^{107}Ag$(p,\gamma)^{108}$Cd reaction using 5 MeV protons. The gray shaded area illustrates the gate onto the $2_1^+ \rightarrow$ g.s. transition with $E_\gamma = 633$ keV. While in the original spectrum (top) many transitions of interest are dominated by background, the gated spectrum (bottom) allows an unambiguous identification of transitions feeding the 2_1^+ state in ^{108}Cd.

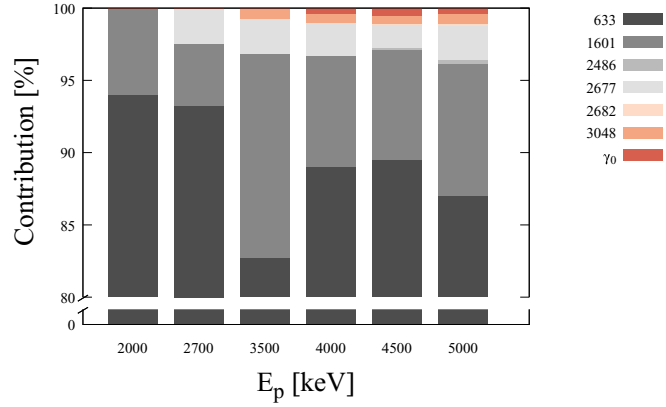

FIG. 6. Contributions of the total ground-state population. By far, the highest contribution stems from the decay of the 2_1^+ state at $E_\gamma = 633$ keV, with about 80%. The relative intensities are almost constant with beam energy.

scattering on ^{107}Ag. In particular, transitions stemming from ^{108}Cd are hardly visible and interfere with the background. The gray shaded area shows the gate onto the $2_1^+ \rightarrow$ g.s. transition with $E_\gamma = 633$ keV in ^{108}Cd, providing the spectrum shown in the lower panel. Many transitions feeding the 2_1^+ state are visible and allow an unambiguous identification. The $\gamma\gamma$-coincidence technique allows one to approximate the influence of various γ-ray transitions on the total cross section. Details on the $\gamma\gamma$-coincidence method can be found in Refs. [30,39].

IV. EXPERIMENTAL CROSS SECTION RESULTS

A. Total cross section

For the population of the ground state and, hence, the determination of total cross sections, the largest contribution stems from the $2_1^+ \rightarrow$ g.s. transition. It yields about 85%, and this share is almost independent of the beam energy (see Fig. 6). Therefore, at lower beam energies, where only a few g.s. transitions were observed, a reliable approximation of an upper limit is possible, assuming the same composition for the ground state population which was extracted from other beam energies.

The total cross-section values obtained in this work are given in Table II and shown in Fig. 7. Energies given are proton energies corrected for the energy loss.

The uncertainties in the cross section values are composed of the uncertainties in the number of projectiles (≈5%), the target thickness (≈10%), full-energy peak efficiency (≈8%), and the statistical error after fitting the Legendre polynomials (≈9%).

We compared the values with a recent measurement from Khaliel *et al.* [40] that was carried out at three proton energies, from which only one data point is in good agreement with the results presented in this work. The deviations between our results and those from Khaliel *et al.* [40] might have various reasons regarding the statistics: In their analysis they took only g.s. transitions from the first two excited states into account. This is shown to be a good assumption solely for lower beam energies (see Fig. 6) and they assumed an

TABLE II. Total and partial cross-section values $\sigma(\gamma_i)$ for the ^{107}Ag$(p,\gamma)^{108}$Cd reaction as a function of beam energy. Except for the 3^+ state at $E_\gamma = 2145$ keV, primary γ-ray transmissions into the first eight excited levels have been observed. Also the excitation energy (E_x), spin (J), and parity (π) are given.

E_x (keV)		0	633	1508	1601	1720	1913	2162	2202
J^π		0^+	2^+	4^+	2^+	0^+	0^+	2^+	3^-
E_p (keV)	σ_{tot} (μb)	$\sigma(\gamma_0)$ (μb)	$\sigma(\gamma_1)$ (μb)	$\sigma(\gamma_2)$ (μb)	$\sigma(\gamma_3)$ (μb)	$\sigma(\gamma_4)$ (μb)	$\sigma(\gamma_5)$ (μb)	$\sigma(\gamma_7)$ (μb)	$\sigma(\gamma_8)$ (μb)
1978 ± 25	0.62 ± 0.09								
2680 ± 25	6.66 ± 0.96								
3487 ± 25	52.2 ± 7.4	0.28 ± 0.04	0.20 ± 0.04		0.10 ± 0.04	0.07 ± 0.02			
3988 ± 25	124 ± 14	0.45 ± 0.17	0.37 ± 0.15	0.06 ± 0.03	0.19 ± 0.08	0.08 ± 0.03	0.16 ± 0.07	0.09 ± 0.04	0.22 ± 0.09
4488 ± 25	278 ± 41	1.42 ± 0.18	1.08 ± 0.14	0.17 ± 0.04	0.39 ± 0.06	0.21 ± 0.04	0.17 ± 0.03	0.21 ± 0.04	0.24 ± 0.04
4991 ± 25	433 ± 53	1.84 ± 0.72	1.38 ± 0.54	0.25 ± 0.10	0.45 ± 0.18	0.35 ± 0.14	0.29 ± 0.12	0.45 ± 0.18	0.48 ± 0.19

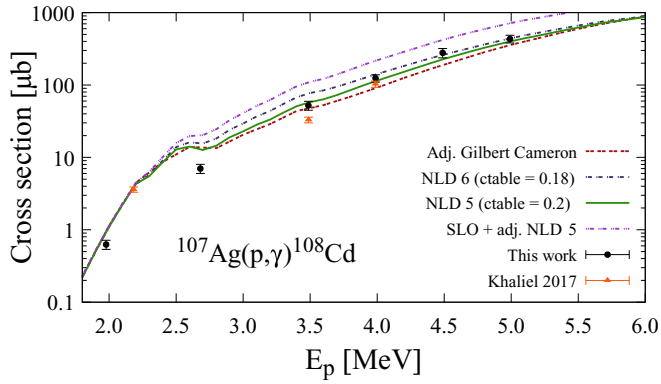

FIG. 7. Results for the total cross-section measurement of the ^{107}Ag(p,γ) ^{108}Cd reaction. The experimental results are compared to statistical model calculations as well as to recently published data from Khaliel *et al.* [40]. Using the microscopic models for the γ-SF from Ref. [59] and the NLD from Refs. [48,50] provides excellent agreement with the experimental values. Both microscopic NLD models have been slightly adjusted in order to obtain better agreement. Similar results are provided by the adjusted Gilbert-Cameron model. See Sec. V for details. Note that the standard Lorentzian [54,55] combined with the adjusted NLD 5 model overestimates the experimental cross sections. The predicted level densities for the NLD models used for the calculations are shown in Fig. 9.

isotropic emission behavior of the γ rays after the proton capture. However, Fig. 2 shows nicely that an angular distribution is observed. We have an excellent setup to minimize the uncertainties due to the high total detection efficiency, longer irradiation times, and larger target thicknesses (about a factor of 4) and, thus, statistics. Furthermore, the usage of highly enriched targets reduces contaminations of the γ-ray spectra, leading to a better identification and analysis of peaks. It is remarkable that, despite these facts, our relative uncertainties for the total cross-section results are larger ($\approx$14% compared to $\approx$9% quoted in Ref. [40]).

B. Partial cross section

Partial cross sections up to the eighth excited state in ^{108}Cd have been observed in this experiment except for the population of the 3^+ state at $E_x = 2145$ keV. This is to be expected as, according to TALYS calculations, mainly 1^-, 1^+, and 2^+ states are populated in the compound nucleus in the ^{107}Ag(p,γ) reaction. The experimentally determined partial cross sections are shown in Table II and Fig. 8 and reveal that the (p,γ_2) cross section is significantly lower than for the other transitions. For the lowest beam energies of $E_p = 2000$ and 2700 keV, primary γ-ray transitions were not observed at all. Notice that the population of the first 4^+ state at $E_\gamma = 1508$ keV $(=\gamma_2)$ is most likely not populated via $E1$ transitions, leading to a strongly reduced intensity. The transmission coefficients for $E1$ and $M1$ transitions can be estimated using the RIPL-2 database and reveal that, at excitation energies of about $E_x \approx 10$ MeV, the electromagnetic deexcitation is heavily dominated by $E1$ transitions (by about one order of magnitude compared to $M1$ transitions) [41]. Therefore, it is reasonable to assume that the direct population of the low-lying 0^+, 2^+, and 3^- states in ^{108}Cd is dominated by $E1$ transitions. The population of 3^+ states via $M1$ transitions is strongly suppressed.

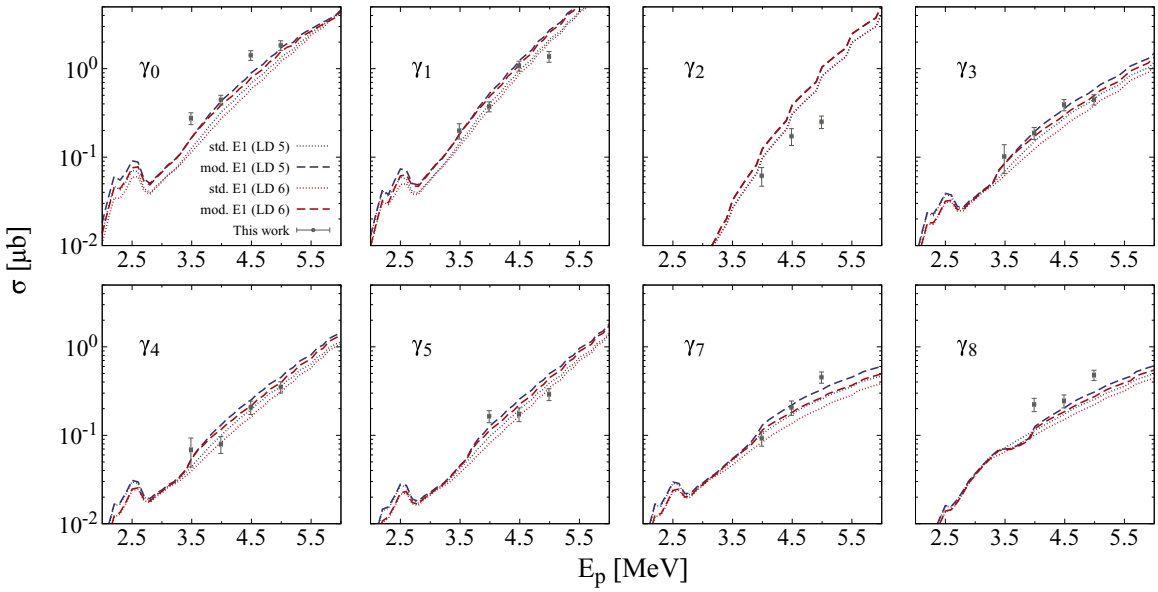

FIG. 8. Experimentally determined partial cross sections of the ^{107}Ag(p,γ) ^{108}Cd reaction compared to theoretical calculations. The default Gogny D1M HFB+QRPA γ-SF (dotted) [59] provides a good reproduction of the experimental values. The adjusted $E1$ strength (dashed) has been used for a better reproduction (see Sec. V C). Furthermore, both microscopic NLD models which have been adjusted via the total cross-section measurement are used. Except for the γ_2 transition all partial cross sections are well described using the adjusted dipole strength and therefore prove that their intensities are predominantly affected by the $E1$ strength function.

V. STATISTICAL MODEL ANALYSIS

The experimental results for the total cross sections are compared to TALYS v1.9 [33] calculations based on different models of nuclear physics input parameters, which shall be now introduced.

The calculated total (p, γ) cross-section values are mostly affected by the chosen models for the NLD, γ-ray strength function (γ-SF), and particle+nucleus OMPs. The well-established proton- and neutron-OMP by Koning and Delaroche [42] provided excellent agreement with many experiments in recent years (see Refs. [26,27] and references therein) and therefore has been used for all calculations. Additionally, the model by Koning and Delaroche has been validated for this reaction via the comparison of calculations to the experimental (p, n) cross section [43], which is almost exclusively sensitive to the proton OMP [44]. Other proton-OMP models that are available in the TALYS code have been tested in the calculations but showed no significant difference. For this reasons, only the NLD and γ-SF models are studied using the (p, γ) cross-section measurements. We will start our analysis as follows: In Sec. V A we investigate the impact of the NLD and compare various NLD models with the low energy level scheme in ^{108}Cd. In Sec. V B we discuss the impact of the change of the total γ-decay width using different γ-SF models. In both of these discussions we will compare the results to recent results from Oslo-type experiments on other Cd isotopes. In Sec. V C we show the investigations of partial decay widths, which give direct access to the γ-ray strength function in ^{108}Cd.

A. Nuclear level density

Theoretical NLD models describe the amount of levels in units of MeV^{-1} and give an average spin-parity distribution. The possibility to average over nuclear properties only becomes available if the amount of levels per energy is sufficiently high, i.e., the level spacing becomes smaller than the average resonance width. A proper NLD model should not only provide reliable predictions about the level density in the continuum, but it should also match with the amount of discrete levels at low energies, which can be extracted from experiments. Hence, we started our analysis by comparing the predictions of NLD models to the cumulative number of levels in ^{108}Cd.

Various models exist for the NLD, ranging from purely phenomenological analytical models to level densities derived from microscopic approaches. More information can be found in Ref. [45]. Actually, for an optimization of the results from calculations using these models, adjustable parameters are used. An analytical formula to predict the spin-dependent NLD is given by the back-shifted Fermi gas model [46] or the Gilbert-Cameron model [47]. Both models feature a Gaussian spin distribution.

For a few years a combinatorial approach based on microscopic Hartree-Fock calculations has been available [48]. The most recent NLD model implemented in TALYS is based on the D1M+Gogny interaction [49] which uses a temperature-dependence to account for changing nuclear properties at higher excitation energies. Moreover, it assumes a non-Gaussian spin distribution [50]. This NLD model is implemented in TALYS 1.8 as ldmodel 6. However, a comparison with experimental data showed slightly higher deviations [49] compared to the phenomenological back-shifted Fermi gas model [46] or the formerly developed microscopic level density based on the Skyrme interaction [48]. The latter is implemented in TALYS 1.8 as ldmodel 5.

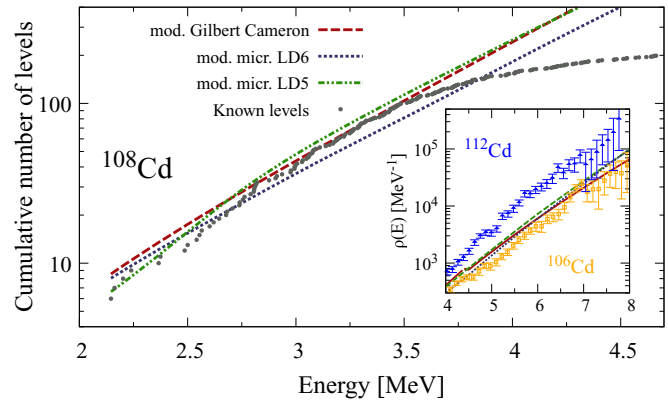

FIG. 9. Cumulative number of levels in ^{108}Cd. Experimentally known levels are marked with circles [34]. The microscopic level densities (green and blue lines) with the adjusted *ctable* parameter describe the values very well. The best agreement for the widely used Gilbert-Cameron model (red) has been achieved by scaling the *nuclear temperature T* by 0.85 and E_0 by 1.30. The inner plot shows the total level density in ^{108}Cd predicted by the aforementioned NLD models. The predicted values fit in the systematics of even-even cadmium isotopes reported in Ref. [51].

For the case of ^{108}Cd, a very good description of the cumulative number of levels is provided by the microscopic approach given by ldmodel 5 (see Fig. 9). As is often the case for microscopic models, adjustment flexibility through a scaling function is provided within the TALYS code and applied for both NLD models for a better reproduction of the experimental values:

$$\rho(E_x, J, \pi) = e^{c\sqrt{E_x - \delta}}\rho_{\mathrm{HFM}}(E_x - \delta, J, \pi), \tag{5}$$

where by default the scaling parameter $c = 0$ and the "pairing shift" δ gives the opportunity to obtain the level density at a different energy, i.e., to shift the NLD. The parameter c is normally obtained from the analysis of the s-wave neutron spacing. More information can be found in Ref. [48]. To improve the agreement between theoretical calculations and experimental results, the c parameter, implemented as ctable in TALYS, has been adjusted for both NLD models in order to achieve a better reconstruction of the total (p, γ) cross-section values. For the Gogny based NLD 6 it was determined to be $ctable = 0.18$ and for the Skyrme based NLD 5 $ctable = 0.2$.

Additionally, we used the model by Gilbert and Cameron [47], which TALYS uses by default when no other specific model is given. The parameters for this model are reported in the RIPL-2 database [41] and can also be found in the TALYS manual [33]. This model with its default parametrization performed poorly for both the cumulative number of levels

and the total (p, γ) cross section. Therefore, this model was adjusted as well in order to reproduce the cumulative number of levels. Basically, the Gilbert and Cameron model features a constant temperature part at low excitation energies with the *nuclear temperature* T and E_0 as adjustable parameters. The best description of the experimental discrete levels was found with scaling factors $a_T = 0.85$ for T and $a_E = 1.30$ for E_0 (see Fig. 9). Note that changes of T and E_0 automatically imply changes to the so-called *matching energy* E_M. At this energy the constant temperature part is matched with the Fermi part of the NLD model.

B. γ-ray strength function and total γ-decay width

All of the aforementioned adjusted NLD models properly describe the cumulative number of levels in ^{108}Cd and they predict very similar results for the total (p, γ) cross section (see Fig. 7). Additionally, they describe the systematics found in even-even cadmium isotopes, which were investigated in Ref. [51] (see the inset of Fig. 9). Hence, we take those models as well-suited input parameters for our following calculations and apply different models for the γ-SF.

The γ-SF holds the information about the properties of the γ-emission channel in nuclear reactions. Since this channel accompanies also emission of almost every other particle, it is important not only for the description of (n, γ) reactions in the s and r processes but also for the nucleosynthesis of p nuclei within the γ process and its huge network of photodisintegration reactions.

Various methods exist to deduce γ-SFs in atomic nuclei. A well-established method is the so-called Oslo method, which can be used to determine γ-SF at low γ-ray energies [52]. Information about the γ-SF built on the ground state can be deduced, for example, by means of the nuclear resonance fluorescence (NRF) method, mostly using bremsstrahlung and monochromatic γ-ray beams for (γ, γ) measurements [53].

The simplest form for describing the giant dipole resonance (GDR) shape is using a standard Lorentzian given by [54,55]. This is commonly used in statistical model calculations for all transitions other than $E1$, hence, this is the default model in TALYS. For $E1$ radiation, it appears that the generalized Lorentzian form of Kopecky and Uhl [56] is more accurate. This model includes an energy-dependent damping width. The first model that was based on a Hartree-Fock Bardeen-Cooper-Schrieffer (HF-BCS) approach [57] aimed at describing the radiative neutron capture cross sections for the whole nuclear chart. Further improvements have been made by introducing a microscopic model using Hartree-Fock for the calculation of the ground state properties combined with the quasiparticle random-phase approximation (QRPA) for the description of the excitation spectrum [58]. The most recent model for the γ-SF uses a state-of-the-art nucleon-nucleon interaction based on the Gogny D1M-QRPA approach [21,49,59]. The main difference of this newest γ-SF compared to former Hartree-Fock-Bogoliubov (HFB)+QRPA models is the implementation of a finite-range Gogny force instead of a zero-range Skyrme force.

The best agreement with the experimental total (p, γ) cross sections is achieved by using the γ-SF from Ref. [59] (Gogny D1M HFB+QRPA). Other models and adjustments for the γ-SF have been tested in the calculations. However, the Gogny D1M HFB+QRPA model is again in great agreement with the systematics of other cadmium isotopes reported in Ref. [51] (see Fig. 10), which is not the case for other (adjusted) γ-SFs, for instance the standard Lorentzian (SLO) [54,55]. The SLO heavily overpredicts the γ-ray transition strength at γ-ray energies from 2 to 6 MeV. This overprediction is inherited to the cross-section calculation, shown in Fig. 7. Hence, we assume that at least for this specific reaction, the Gogny D1M-QRPA γ-SF model is satisfyingly well determined in the energy range that is relevant for the radiative proton capture reaction (approximately 4 to 10 MeV).

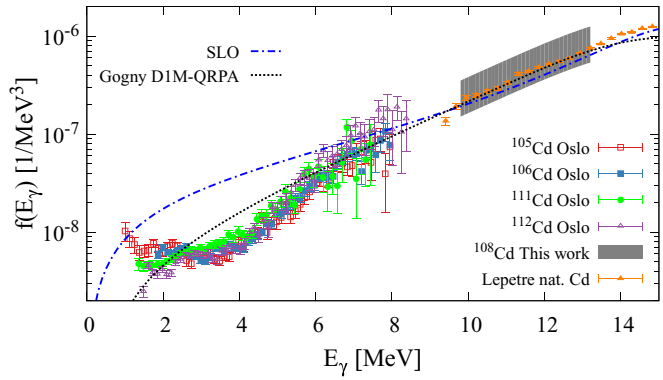

FIG. 10. Extracted $E1$ strength distribution in ^{108}Cd compared to other Cd isotopes. The error band includes the uncertainty for the NLD. The γ-ray strength functions for the Cd isotopes ^{105,106,111,112}Cd were extracted using the Oslo method [51]. Furthermore, photoabsorption cross-section results of natural cadmium from Ref. [65] have been used to determine the γ-ray strength function. The Gogny D1M HFB+QRPA model is in excellent agreement with the systematics of other cadmium isotopes.

The results above show that a NLD model that properly describes the experimentally determined number of levels combined with the Gogny D1M-QRPA γ-SF is able to reproduce the total (p, γ) cross section on ^{107}Ag. Note that no adjustments were applied to this γ-SF. Nevertheless, via the partial cross-section measurement we get access to information about the γ-SF at energiesof $\approx$10 MeV.

C. γ-ray strength function and partial γ-decay width

Assuming that the total (p, γ) cross section is adequately described by the NLD model and p-OMP (see Fig. 7), deviations in the partial cross sections can be tracked back to the γ-SF and are directly proportional to the latter value. To fortify this assumption, we determined the sensitivity of primary γ-ray transitions predicted by TALYS to variations of the NLD model. Figure 11 shows the experimental γ_0 cross sections along with TALYS calculations using various NLD models and the Gogny D1M-QRPA γ-SF. In detail, the various NLD models predict level densities that differ by a factor of about 2 at an excitation energy of 10 MeV. It becomes clear that the uncertainties governed by the NLD are very small, and hence partial cross sections are well suited for studies of the γ-ray strength function (γ-SF). This is also

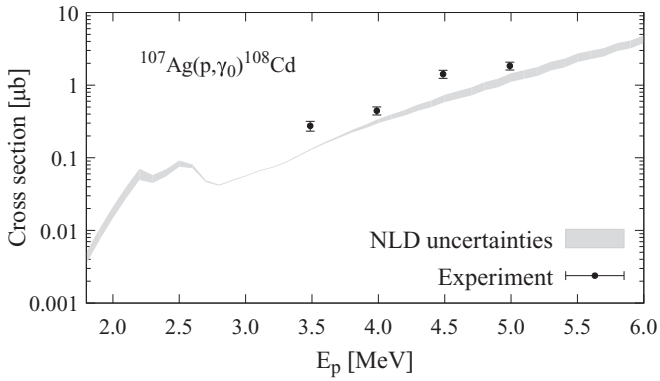

FIG. 11. The partial $^{107}\mathrm{Ag}(p,\gamma_0)^{108}\mathrm{Cd}$ cross section compared to statistical model calculations using all NLD models available in the TALYS code as well as our modified NLD models (gray-shaded area). The cross section for the γ_0 transition is insensitive to different NLD models. The same behavior was found for all other partial cross sections and also for other reactions [28].

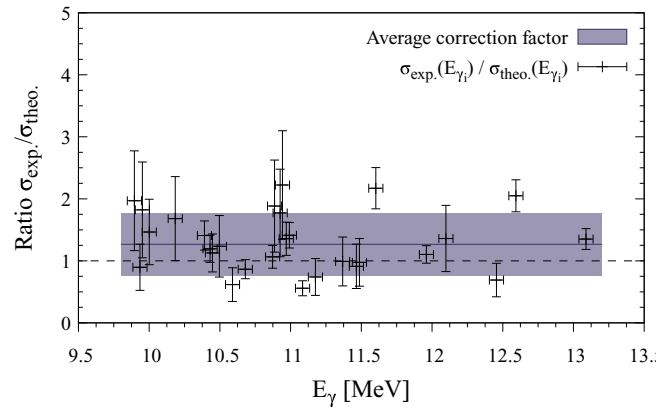

FIG. 12. Determined ratios between experimental partial cross sections and calculations from TALYS. The latter ones are based on the adjusted ldmodel 5 (see Sec. V A) and the Gogny-D1M QRPA γ-ray strength function [59]. Each cross-section ratio is plotted at its respective γ-ray energy. The deviations between experimental and calculated cross sections are predominantly affected by the γ-ray strength function.

discussed in Ref. [60] and used for the experimental analysis of the $^{89}\mathrm{Y}(p,\gamma)^{90}\mathrm{Zr}$ reaction in Ref. [28]. The latter one discusses an experiment similar to that reported in this paper; however, due to space restrictions the explicit steps of the analysis are not described in detail and will be explained in the following.

In general, the strength $f(E_\gamma)$ of primary γ-ray transitions between an energy region E_i in the continuum and a discrete level with energy E_f is given by the expression

$$f_{J^\pi}(E_\gamma) = \frac{\tilde{\Gamma}_{J^\pi}(E_i, E_\gamma)\rho_{J^\pi}(E_i)}{E_\gamma^{2l+1}}, \tag{6}$$

with $\tilde{\Gamma}_{J^\pi}(E_i, E_\gamma)$ the average decay width of γ rays with energy E_γ from levels with spin and parity J^π, ρ_{J^π} the level density at E_i, and l the multipolarity of the transitions. $\tilde{\Gamma}_{J^\pi}(E_i, E_\gamma)$ plays a crucial role for the calculation of partial cross sections in the Hauser-Feshbach model.

Although the Gogny D1M-QRPA dipole strength function already yields very good agreement with the partial cross-section values, the dipole-strength function mentioned above has been adjusted individually via

$$f_{\mathrm{adj}}(E_\gamma) = f_0(E_\gamma)\frac{\sigma(\gamma_i)_{\mathrm{exp.}}}{\sigma(\gamma_i)_{\mathrm{theo.}}}, \tag{7}$$

where $f_0(E_\gamma)$ denotes the original value of the γ-SF, $\sigma_{\mathrm{exp.}}$ the experimentally determined partial cross section, and $\sigma_{\mathrm{theo.}}$ the theoretically calculated partial cross section for the different γ-ray transitions γ_i with their specific energies. As shown in Ref. [28] for ^{90}Zr, this comparison will reveal systematic under- or overpredictions of the γ-ray SF by the respective model for the γ-ray energy region of the direct deexcitation measure in this experiment. As already mentioned above, we assume that the dipole strength function mainly consists of electric dipole character. We confirmed this assumption by applying variations to the $M1$ strength function which showed no significant impact on the partial cross sections.

This analysis was carried out based on the Brink-Axel hypothesis [55,61,62]. This states that the γ-SF is independent of the properties of the initial and final states and should be the same for γ emission and absorption. Furthermore, the γ-ray transmission probability is claimed to be exclusively dependent on the γ-ray energy and is independent of excitation energy. As an example, the γ_0 transition of the 5000 keV measurement provides information about the γ-SF at

$$E_\gamma = Q + E_p - E_x = 13\,134\ \mathrm{keV}. \tag{8}$$

The determined cross-section ratios $\sigma(\gamma_i)_{\mathrm{exp.}}/\sigma(\gamma_i)_{\mathrm{theo.}}$ are shown at their specific γ-ray energies in Fig. 12. Most experimental partial cross sections are systematically underpredicted and show slight fluctuations. Since we cannot certainly say if these fluctuations are caused by fluctuations of the γ-ray strength or by the high statistical uncertainties of the data points, we calculated an average correction factor. Subsequently, we scaled the γ-ray strength function by the correction factor of 1.27 ± 0.48. The recalculated partial cross sections using the adjusted $E1$ strength are shown in Fig. 8. Each partial cross section is calculated with both adjusted NLD models derived from the total cross section analysis in Sec. V A. Furthermore, the original parametrization for the Gogny D1M HFB + QRPA $E1$ strength has been used as well as the adjusted one. The final γ-SF extracted from the partial cross-section measurement is shown in Fig. 10. In the energy range from $E_\gamma = 9.9$ MeV to $E_\gamma = 13.1$ MeV the total $E1$ strength was modified, whereas the lower limit is mainly given by the Q value of 8134 keV. As outlined before, an average correction factor for the $E1$ strength was used; however, recent experiments revealed that fine structure in the low-energy tail of the GDR occur in other nuclei, as reported in Refs. [63,64]. However, in the present case, the precision of the experimental data points was not sufficiently high to draw similar conclusions. In contrast to the $^{89}\mathrm{Y}(p,\gamma)^{90}\mathrm{Zr}$ reaction, only a

slight increase of the high-energy transition strength can be observed [28] and the Gogny D1M HFB+QRPA $E1$ strength in its original parametrization yields a very good interpolation between the adjusted values. Finally, a recalculation of the total (p,γ) cross section with the extracted γ-SF shows no significant changes.

Unfortunately, there are no other experimentally determined data for γ-SFs or NLDs in ^{108}Cd to compare and review the obtained results in this work. However, an experiment applying the Oslo method [52] led to the experimental extraction of NLDs and γ-SFs in other cadmium isotopes, namely ^{105,106,111,112}Cd [51]. The extracted γ-ray strength functions for the four cadmium isotopes using the Oslo method as well as the results obtained in this work are also shown in Fig. 10. Moreover, the photoabsorption cross section results from Ref. [65] have been included in the comparison. The results are in quite good agreement with each other and confirm the assumption that at higher energies the total strength is dominated by the $E1$ strength. It is shown that the Gogny D1M-QRPA $E1$ model [59] is a well-suited choice for the γ-ray SF.

The method of using partial cross-section measurements to constrain the γ-SF brings some restrictions: On the one hand, partial cross sections often have a much smaller intensity compared to the total cross section. Hence, the obtained statistics has a huge impact on the quality of the results. Further improvements of detection efficiency as well as a reliable and stable particle beam of high intensity are crucial for future experiments. Also, measuring at higher beam energies improves the situation significantly. This leads to the consideration of measuring at higher beam energies in small steps, in the order of 100 keV. Another approach is to measure at low energies with the focus on the strongest transitions, e.g., γ_0 or γ_1. Independently of the experimental approach, the final restriction on the energy range that can be investigated is given by the Q value of the reaction that is studied.

VI. SUMMARY AND CONCLUSION

In this paper total and partial cross section results of the radiative proton-capture reaction ^{107}Ag$(p,\gamma)^{108}$Cd for beam energies $2.0 < E_p < 5.0$ MeV were presented. The results allow for an improvement of the underlying nuclear-physics models for statistical model calculations in nuclear astrophysics. Essentially, the total (p,γ) cross section is affected by the nuclear level density (NLD) and the total γ-decay width above the (p,n) threshold whereas partial cross sections are heavily dominated by the exact energy dependence of the γ-ray strength function (γ-SF). These are two of the main ingredients for Hauser-Feshbach calculations, not only for the p-process nucleosynthesis but also for the calculation of s- and r-process reaction rates. The total cross sections were compared to statistical model calculations to constrain the NLD model. Two microscopic NLD models ("NLD 5" [48] and "NLD 6" [50]) based on HFB+combinatorial calculations had to be slightly adjusted in order to provide an excellent agreement between experimental data and theory. No huge differences could be found between the two NLD models and they were used in parallel for all following calculations.

The γ-ray spectrometer HORUS is also suitable for partial cross-section measurements. Since those are very sensitive to the γ-SF it was possible to obtain an adjusted $E1$ strength distribution in ^{108}Cd based on the microscopic Gogny D1M HFB + QRPA model [59]. After the (p,γ) reaction the excited compound nucleus predominantly deexcites via $E1$ transitions into different levels in ^{108}Cd. The comparison of experimental partial cross sections and theoretical calculations allowed the adjustment of the $E1$ strength between $E_\gamma = 9.9$ MeV and $E_\gamma = 13.1$ MeV. The adjusted γ-ray SF values revealed no significant under- or overprediction by the γ-ray SF model (Gogny D1M) but the ratio between experimental and theoretical partial cross sections exhibits some fluctuations. These can be caused by real fluctuations in the γ-ray SF. However, we presume that the very low cross sections, and hence the large statistical uncertainties for the partial cross sections do not allow us to draw any further conclusions. The Gogny D1M HFB+QRPA $E1$ strength function in its default parametrization also yields excellent agreement with the total and partial cross section results and proves to be a reliable choice for the γ-ray SF in the present case.

In summary, the method of using total and partial cross sections for the study of nuclear level densities and γ-ray strength functions shows very promising results. This method provides an insight into the statistical γ-decay behavior of ^{108}Cd and, similarly to the Oslo method, allows one to indirectly determine the NLD and γ-SF. Note that we do not draw any deeper conclusions about the models we start our calculations with.

Our understanding of the nuclear-physics models for Hauser-Feshbach statistical calculations, especially in the Sn-Cd region, has been expanded by the latest experiments [27–29]. In the future, the extraction of γ-SFs and NLDs via proton-capture reactions will be addressed further. In particular, experiments have been already performed to study the nuclei ^{110}Cd, ^{94}Mo, and ^{64,66}Zn. For the case of ^{94}Mo other γ-SF data and NLD data are available for a comparison [66] and for the case of ^{110}Cd we will study how the extracted models presented in this work behave systematically (similar to the results shown in Fig. 10).

Additionally, we would like to emphasize the importance of global and robust models for theoretical predictions of astrophysical properties. Therefore, detailed studies of all kind of nuclear properties need to be further addressed, combined with a careful interpretation.

ACKNOWLEDGMENTS

The authors acknowledge the help of the accelerator staff at the Institute for Nuclear Physics in Cologne for providing excellent beams. Moreover, we gratefully thank K. O. Zell and A. Blazhev for the target preparation and H.W. Becker of the Ruhr-Universität Bochum for the assistance during the RBS measurements. We thank S. Goriely from the University of Brussels for his valuable help and advice for the study of the NLD and γ-SF. This project has been supported by the

Deutsche Forschungsgemeinschaft (DFG) under the contracts ZI 510/7-1 and INST 216/544-1 and the emerging group ULDETIS within the UoC Excellence Initiative institutional strategy.

[1] E. M. Burbidge, G. R. Burbidge, W. A. Fowler, and F. Hoyle, Rev. Mod. Phys. **29**, 547 (1957).
[2] M. Arnould, S. Goriely, and K. Takahashi, Phys. Rep. **450**, 97 (2007).
[3] F. Käppeler, R. Gallino, S. Bisterzo, and W. Aoki, Rev. Mod. Phys. **83**, 157 (2011).
[4] M. Pignatari, R. Gallino, M. Heil, M. Wiescher, F. Käppeler, F. Herwig, and S. Bisterzo, Astrophys. J. **710**, 1557 (2010).
[5] M. Pignatari, K. Göbel, R. Reifarth, and C. Travaglio, Int. J. Mod. Phys. E **25**, 04 (2016).
[6] Zs. Nêmeth, F. Käppeler, C. Theis, T. Belgya, and S. W. Yates, Astrophys. J. **426**, 357 (1994).
[7] C. Arlandini, F. Käppeler, K. Wisshak, R. Gallino, M. Lugaro, M. Busso, and O. Straniero, Astrophys. J. **525**, 886 (1999).
[8] M. Arnould and S. Goriely, Phys. Rep. **384**, 1 (2003).
[9] T. Rauscher, N. Dauphas, I. Dillmann, C. Fröhlich, Zs. Fülöp, and Gy. Gyürky, Rep. Prog. Phys. **76**, 066201 (2013).
[10] W. Rapp, J. Görres, M. Wiescher, H. Schatz, and F. Käppeler, Astrophys. J. **653**, 474 (2006).
[11] S. E. Woosley and W. M. Howard, Astrophys. J. Suppl. **36**, 285 (1978).
[12] M. Rayet, M. Arnould, M. Hashimoto, N. Prantzos, and K. Nomoto, Astron. Astrophys. **298**, 517 (1995).
[13] T. Rauscher, A. Heger, R. D. Hoffman, and S. E. Woosley, Astrophys. J. **576**, 323 (2002).
[14] S. E. Woosley and A. Heger, Phys. Rep. **442**, 269 (2007).
[15] C. Travaglio, F. K. Röpke, R. Gallino, and W. Hillebrandt, Astrophys. J. **739**, 93 (2011).
[16] T. Rauscher, Phys. Rev. C **73**, 015804 (2006).
[17] A. Parikh, J. Jos, G. Sala, and C. Iliadis, Prog. Part. Nucl. Phys. **69**, 225 (2013).
[18] H. Schatz, A. Aprahamian, J. Görres *et al.*, Phys. Rep. **294**, 167 (1998).
[19] R. K. Wallace and S. E. Woosley, Astrophys. J. Suppl. **45**, 389 (1981).
[20] C. Fröhlich, G. Martinez-Pinedo, M. Liebendörfer, F.-K. Thielemann, E. Bravo, W. R. Hix, K. Langanke, and N. T. Zinner, Phys. Rev. Lett. **96**, 142502 (2006).
[21] S. Goriely, Eur. Phys. J. A **51**, 172 (2015)
[22] H. Schatz, J. Phys. G: Nucl. Part. Phys. **43**, 064001 (2016).
[23] W. Hauser and H. Feshbach, Phys. Rev. **87**, 366 (1952).
[24] T. Rauscher and F.-K. Thielemann, At. Data Nucl. Data Tables **75**, 1 (2000).
[25] T. Rauscher, Int. J. Mod. Phys. E **20**, 5 (2011).
[26] L. Netterdon, J. Mayer, P. Scholz, and A. Zilges, Phys. Rev. C **91**, 035801 (2015).
[27] P. Scholz, F. Heim, J. Mayer, C. Münker, L. Netterdon, F. Wombacher, and A. Zilges, Phys. Lett. B **761**, 247 (2016).
[28] L. Netterdon, A. Endres, S. Goriely, J. Mayer, P. Scholz, M. Spieker, and A. Zilges, Phys. Lett. B **744**, 358 (2015).
[29] J. Mayer, S. Goriely, L. Netterdon, S. Peru, P. Scholz, R. Schwengner, and A. Zilges, Phys. Rev. C **93**, 045809 (2016).
[30] A. Sauerwein, J. Endres, L. Netterdon, A. Zilges, V. Foteinou, G. Provatas, T. Konstantinopoulos, M. Axiotis, S. F. Ashley, S. Harissopulos, and T. Rauscher, Phys. Rev. C **86**, 035802 (2012).
[31] S. Harissopulos, A. Spyrou, A. Lagoyannis, M. Axiotis, P. Demetriou, J. W. Hammer, R. Kunz, and H.-W. Becker, Phys. Rev. C **87**, 025806 (2013).
[32] Gy. Gyürky, Zs. Fülöp, F. Käppeler, G. G. Kiss, and A. Wallner, Eur. Phys. J. A **55**, 41 (2019).
[33] A. Koning and D. Rochman, Nucl. Data Sheets **113**, 2841 (2012).
[34] J. Blachot, Nucl. Data Sheets **91**, 135 (2000).
[35] J. Brenneisen, D. Grathwohl, M. Lickert, R. Ott, H. Röpke, J. Schmälzlin, P. Siedle, and B. H. Wildenthal, Z. Phys. A: Hadrons Nucl. **352**, 149 (1995).
[36] M. Mayer, in *the Fifteenth International Conference on the Application of Accelerators in Research and Industry*, 4–7 November 1998, Denton, TX, edited by J. L. Duggan, B. Stippec, and I. L. Morgan, AIP Conf. Proc. No. 475 (AIP, New York, 1999), p. 541.
[37] J. Ziegler, J. Biersack, and M. Ziegler, SRIM - The Stopping and Range of Ions in Matter, http://srim.org/
[38] L. Netterdon, V. Derya, J. Endres, C. Fransen, A. Hennig, J. Mayer, C. Müller-Gatermann, A. Sauerwein, P. Scholz, M. Spieker, and A. Zilges, Nucl. Instrum. Methods Phys. Res., Sect. A **754**, 94 (2014).
[39] P. Scholz *et al.*, Phys. Rev. C **90**, 065807 (2014).
[40] A. Khaliel, T. J. Mertzimekis, E.-M. Asimakopoulou, A. Kanellakopoulos, V. Lagaki, A. Psaltis, I. Psyrra, and E. Mavrommatis, Phys. Rev. C **96**, 035806 (2017).
[41] R. Capote *et al.*, Nucl. Data Sheets **110**, 3107 (2009).
[42] A. Koning and J. Delaroche, Nucl. Phys. A **713**, 231 (2003).
[43] R. L. Hershberger, D. S. Flynn, F. Gabbard, and C. H. Johnson, Phys. Rev. C **21**, 896 (1980).
[44] T. Rauscher, Astrophys. J. Suppl. **201**, 26 (2012).
[45] A. Koning, S. Hilaire, and S. Goriely, Nucl. Phys. A **810**, 13 (2008).
[46] W. Dilg, W. Schantl, H. Vonach, and M. Uhl, Nucl. Phys. A **217**, 269 (1973).
[47] A. Gilbert and A. G. W. Cameron, Can. J. Phys. **43**, 1446 (1965).
[48] S. Hilaire and S. Goriely, Nucl. Phys. A **779**, 63 (2006).
[49] S. Goriely, S. Hilaire, M. Girod, and S. Peru, Phys. Rev. Lett. **102**, 242501 (2009).
[50] S. Hilaire, M. Girod, S. Goriely, and A. J. Koning, Phys. Rev. C **86**, 064317 (2012).
[51] A. C. Larsen *et al.*, Phys. Rev. C **87**, 014319 (2013).
[52] A. Schiller, B. L., M. Guttormsen, E. Melby, J. Rekstad, and S. Siem, Nucl. Instrum. Methods Phys. Res., Sect. A **447**, 498 (2000).
[53] D. Savran, T. Aumann, and A. Zilges, Prog. Part. Nucl. Phys. **70**, 210 (2013).
[54] D. Brink, Nucl. Phys. **4**, 215 (1957).
[55] P. Axel, Phys. Rev. **126**, 671 (1962).
[56] J. Kopecky and M. Uhl, Phys. Rev. C **41**, 1941 (1990).
[57] S. Goriely and E. Khan, Nucl. Phys. A **706**, 217 (2002).

[58] S. Goriely, E. Khan, and M. Samyn, Nucl. Phys. A **739**, 331 (2004).
[59] M. Martini, S. Peru, S. Hilaire, S. Goriely, and F. Lechaftois, Phys. Rev. C **94**, 014304 (2016).
[60] M. Wiedeking *et al.*, Phys. Rev. Lett. **108**, 162503 (2012).
[61] D. Brink, Ph.d. thesis, Oxford University, 1955 (unpublished).
[62] M. Guttormsen, A. C. Larsen, A. Gorgen, T. Renstrom, S. Siem, T. G. Tornyi, and G. M. Tveten, Phys. Rev. Lett. **116**, 012502 (2016).
[63] I. Poltoratska, R. W. Fearick, A. M. Krumbholz, E. Litvinova, H. Matsubara, P. von Neumann-Cosel, V. Yu. Ponomarev, A. Richter, and A. Tamii, Phys. Rev. C **89**, 054322 (2014).
[64] R. W. Fearick, B. Erler, H. Matsubara, P. von Neumann-Cosel, A. Richter, R. Roth, and A. Tamii, Phys. Rev. C **97**, 044325 (2018).
[65] A. Lepêtre, H. Beil, R. Bergre, P. Carlos, A. De Miniac, A. Veyssire, and K. Kernbach, Nucl. Phys. A **219**, 39 (1974).
[66] H. Utsunomiya *et al.*, Phys. Rev. C **88**, 015805 (2013).